GENERATION OF TYPE III SOLAR RADIO BURSTS IN THE LOW CORONA BY DIRECT AMPLIFICATION

C. S. WU,[1,2] C. B. WANG,[1] PETER H. YOON,[2] H. N. ZHENG,[1] AND S. WANG[1]

ABSTRACT

An alternative scenario to the plasma-emission model is proposed for coronal type III solar radio bursts. According to this model, the radio bursts are produced inside a magnetic flux tube with density depletion by a direct amplification of electromagnetic waves with frequencies near the electron gyrofrequency and its harmonics. The amplification mechanism is the cyclotron-maser instability driven by a beam of flare-generated streaming electrons. In the present discussion, a depletion factor of approximately 10^2 near the chromosphere is assumed. The essential point is that in order to produce the electromagnetic waves near the fundamental electron gyrofrequency, the present model requires $0.1 \leq f_p/f_g \leq 0.4$ (where f_p and f_g denote the plasma frequency and gyrofrequency, respectively) in the source region. The propagation of an amplified wave is initially confined within the magnetic flux tube until the wave arrives at a point where the local exterior cutoff frequency is equal to the exiting wave frequency. The proposed model is spurred by the consideration that above an active region where the emission is presumed to originate, the ambient magnetic field is strong enough that, in contrast to conventional theories, it cannot be ignored. Preliminary analysis leads to some encouraging results, on the basis of which we may resolve a number of long-standing issues raised by observations. The proposed scenario also implies a fundamentally different interpretation of the observed frequency drift in the dynamic spectrum.

Subject headings: masers — plasmas — Sun: radio radiation

1. INTRODUCTION

Type III solar radio emission has been studied and discussed extensively by many authors during the past several decades. The central issue is how a beam of fast electrons leads to the generation of electromagnetic waves with frequencies close to the local plasma frequency (i.e., plasma emission), as suggested by observations. A pioneering theory put forth to explain the observed fundamental (F) and harmonic (H) bands was proposed by Ginzburg & Zheleznyakov (1958). Further discussions on this topic emerged in subsequent years (e.g., see reviews by Goldman 1983 and Melrose 1985 for early theoretical efforts).

More recent discussions of refined plasma-emission models can also be found in works by Cairns (1987a, 1987b, 1987c), Robinson & Cairns (1994, 1998a, 1998b, 1998c), Robinson, Willes, & Cairns (1993), Robinson, Cairns, & Willes (1994), Willes, Robinson, & Melrose (1996), Wu, Yoon, & Zhou (1994), Yoon & Wu (1994), and Yoon (1995, 1997, 1998). Among these theories, Robinson, Cairns, and their coworkers proposed the stochastic-growth theory, culminating in a three-part series (Robinson & Cairns 1998a, 1998b, 1998c). These authors address a number of outstanding issues that had not been satisfactorily accounted for on the basis of early theories. Lately, this model has also been applied to bidirectional type III bursts (Robinson & Benz 2000).

In the plasma-emission theory, the beam-generated Langmuir waves play a pivotal role. The differences in existing theories are only in the details by which the excited Langmuir waves are partly converted to electromagnetic waves,

but invariably they all assume that the source region of type III bursts is characterized by a very weak ambient magnetic field, so that its effects on the emission process can be ignored. Although this approximation may be justified for source regions sufficiently far away from the Sun, it is not obvious that it is appropriate for the emissions taking place near an active region in the low corona where the electrons are strongly magnetized. There is observational evidence that type III bursts (as well as several other types of solar radio emissions) are indeed produced in these regions (Kai, Melrose, & Suzuki 1985; Suzuki & Dulk 1985; Poquerusse & McIntosh 1995).

The notion that motivates the present discussion is that near an active region, direct emission of radiation is possible via a cyclotron-maser instability mechanism, which is the known emission mechanism for the Earth's auroral kilometric radiation and other planetary radio emissions. The purpose of the present paper is to report some preliminary findings from our recent efforts. Since the physics of the cyclotron-maser instability is fairly well known, we minimize theoretical details and only provide some calculations relevant to observations. The organization of the paper is as follows: In § 2 basic considerations relevant to the proposed model are discussed. Then, the emission model is described in § 3. In §§ 4–6 we present the discussion and concluding remarks.

2. SOME BASIC CONSIDERATIONS

2.1. *Duct with Density Depletion*

Among the observed features associated with both type II and III bursts, the occasional occurrence of two emission bands (Wild, Murray, & Rowe 1954) had a great impact on the development of theoretical models. Because at a given time the two bands have a frequency ratio approximately

[1] Department of Earth and Space Sciences, University of Science and Technology of China, Hefei, Anhui 230026, China.
[2] Institute for Physical Science and Technology, University of Maryland, College Park, MD 20742.

equal to 2, it is postulated that one is the fundamental (F) component, with frequencies close to the local plasma frequency (f_p), while the other represents the harmonic (H) component, with frequencies close to $2f_p$.

Early theories assumed that these waves are generated in the same source region. However, subsequent observational studies raised doubts about this interpretation (Smerd, Wild, & Sheridan 1962; Bougeret et al. 1970; McLean 1971; Stewart 1972, 1974a; Mercier & Rosenberg 1974; Rosenberg 1975; Daigne 1975a, 1975b; Dulk & Suzuki 1980). It is found that F- and H-band waves observed at a fixed frequency occupy the same apparent source positions (Smerd et al. 1962; McLean 1971; Stewart 1972, 1974a, 1974b; Dulk & Suzuki 1980), which is not immediately compatible with the plasma-emission model. This finding prompted several researchers to propose scattering and group delay as possible causes (Steinberg et al. 1971; Riddle 1972, 1974; Leblanc 1973), but these are generally not satisfactory (Suzuki & Dulk 1985).

Two subsequently proposed ideas deserve mention. First, Duncan (1979) noted that if the emission of waves takes place inside an underdense duct where the interior density is at least 4 times less than the exterior density, then F- and H-component waves with the same frequency would exit the duct at the same altitude. The second scenario, proposed by Robinson (1983), stresses that overdense density fibers may result in wave scattering that tends to shift the apparent source heights of both the F and H components. These effects were further elaborated in several papers (Bougeret & Steinberg 1977; Roelof & Pick 1989; Benz 1993; Poquerusse & McIntosh 1995).

The notion that underdense and overdense flux tubes exist in solar corona grew out of the data acquired with white-light coronagraphs or soft X-ray images that show fibrous density structures extending over a large distance. Physically, such a density corrugation can be understood from the fact that the plasma beta in the corona is generally very low. As a result, small magnetic field variation in the transverse direction can result in large density variation perpendicular to the magnetic field, while the plasma density along the field lines remains smooth. The model to be discussed in this paper emphasizes the effect of underdense ducts. However, our model postulates that the interior density is much lower than that implied by Duncan (1979).

2.2. *The Ratio f_p/f_g in a Density-depleted Duct*

It turns out that the ratio f_p/f_g (where f_p and f_g denote the plasma frequency and electron gyrofrequency, respectively) is an important parameter in the model to be discussed. For this reason, a discussion of the density and magnetic field models is necessary.

Numerous models for the electron density profile in the corona are available in the literature, as reviewed by Newkirk (1967), Dulk (1985), and McLean (1985). A recent study by Aschwanden & Benz (1997) also gives a detailed discussion of electron density near a flare site. Their discussion covers the acceleration sites but is restricted to low altitudes, and they infer the electron density on the basis of radio observations, assuming that the emission frequency is at the local plasma frequency.

In our model, the coronal electron density n_0 (i.e., the electron density exterior to the duct) above an active region is assumed to be

$$n_0(R) = 10^9 R^{-6} \text{ cm}^{-3} , \qquad (1)$$

which qualitatively corresponds to the Newkirk model in the low corona (Newkirk 1967). Within the density-depleted duct, the electron density n is postulated as

$$n(R) = \frac{n_0(R)}{10^2 g(R) + 1} ,$$
$$g(R) = 1 - \tanh\left(\frac{R - 5}{2}\right) , \qquad (2)$$

where in equations (1) and (2), R is the distance measured from the center of the Sun in units of $R_\odot$. Expression (2) reflects the fact that the density at low altitudes is depleted by a factor of 10^{-2}. The analytic expressions (1) and (2) are introduced to facilitate the analysis and calculations to be discussed later.

The subject of solar magnetic fields is reviewed in a number of publications (e.g., Zirin 1966; Zheleznyakov 1970; Newkirk 1967, 1971; Dulk & McLean 1978) from which the reader may realize that to model the magnetic field in regions of interest to us is by no means easy. Near an active region, the magnetic fields usually have very complex structures. Moreover, the local magnetic field near a leading sunspot could be many times higher than the average magnetic field at the same altitude elsewhere. Owing to the localized nature of an active region, a simple magnetic field model as a function of altitude is not possible. All available magnetic field models are inferred from indirect measurements that include radio observations of type II and type V bursts. Because theoretical understanding of these radio phenomena is still limited to this date, uncertainties are inevitable in all available models.

Our discussion is merely concerned with the variation of the magnetic field along the path of the electron beam. Considering open field lines emanating from an active region, we choose to adopt the Newkirk model (Newkirk 1967, 1971). Since type I and type III bursts are believed to be generated in regions above a leading sunspot, we postulate that a model with a strong magnetic field may be appropriate. It is based on this consideration that the choice is made. The model magnetic field B and the density profile exterior to the duct, n_0, are shown in Figure 1, in which these quantities are plotted as a function of distance R, normalized to the solar radius.

Here we remark that the choice of interior density model described by equation (2) is based on two basic considerations: First, according to observations, F-H pair emission usually occurs in a frequency range corresponding to a few MHz $< f \le 200$ MHz (Suzuki & Dulk 1985). It turns out that the optimum range of f_p/f_g for the operation of maser instability is $0.1 \le f_p/f_g \le 0.3$, as is discussed in § 3. Thus, we have manipulated the density depletion factor so that f_p/f_g remains in the range $0.1 \le f_p/f_g \le 0.3$ over the altitudes where the local gyrofrequency varies from 200 down to a few MHz. Second, as is discussed in § 5, the maximum interior plasma frequency, which occurs at the bottom of the corona, may represent the highest frequency of a type V emission event. It is well known that type V emission tends to diminish progressively as the frequency increases. The peak frequency varies from a few tens of MHz to about 100 MHz. In the present case, we arbitrarily choose 30 MHz
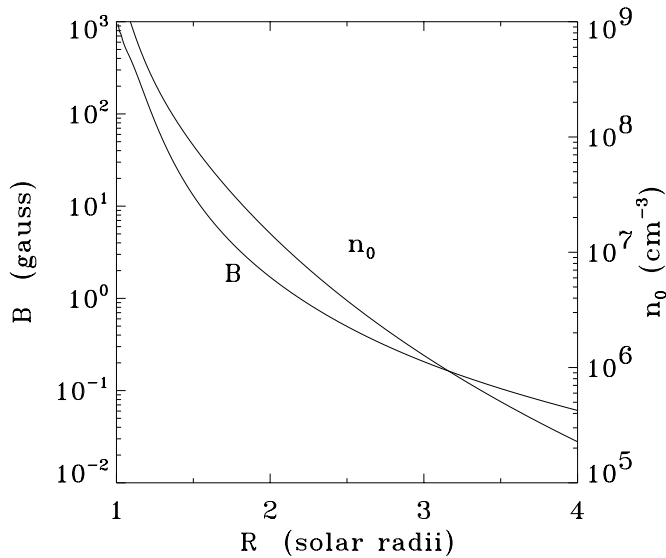
FIG. 1.—Assumed magnetic field and electron density profiles vs. radial distance R.

to signify the highest interior plasma frequency. (We could also consider a higher frequency [but below 100 MHz] and yet still fulfill the first requirement, provided that the functional form of eq. [2] is appropriately modeled.) Here we stress that the density and magnetic field models are considered mainly for the purpose of illustration.

In Figure 2 we show the ratio f_p/f_g, computed on the basis of the model magnetic field and density, versus R. The quantity f_{p0}/f_g represents the frequency ratio corresponding to the exterior region, while f_p/f_g represents the same ratio within the density-depleted duct. Note that f_p/f_g indeed remains lower than 0.5 over the altitude range $1 < R < 2$.
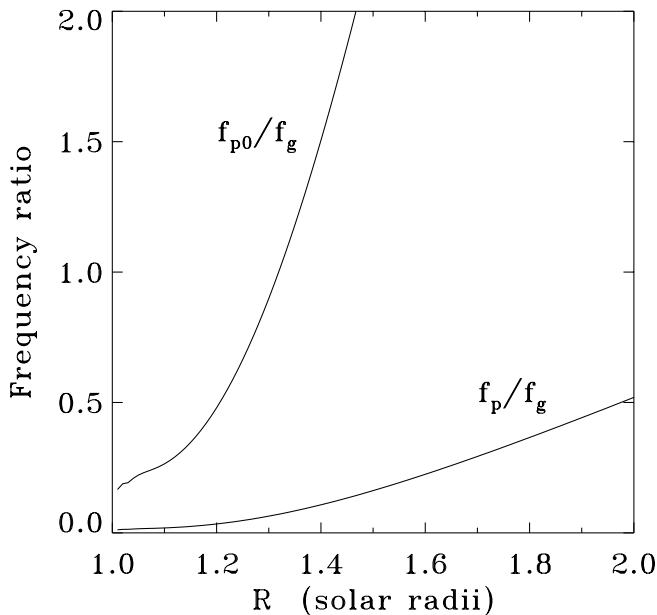
FIG. 2.—Ratio of the plasma frequency to the gyrofrequency vs. radial distance R. Here, f_{p0} and f_p denote the plasma frequency outside and inside the duct, respectively, and f_g is the electron gyrofrequency.

3. THE GENERATION OF OBSERVED RADIATION

The purpose of this section is to describe a maser-beam instability that can lead to direct amplification of high-frequency electromagnetic waves. We suggest that type III solar radio emission in the low corona is produced via this process.

It is believed that enhanced Alfvén waves exist pervasively in the solar corona. Our model assumes that these waves can pitch-angle scatter the streaming electrons. The pitch-angle scattering is more effective for fast electrons. The basic physical picture is as follows: while a streaming electron moves along the ambient magnetic field with speed v_b and interacts with a wave field δB_W, it experiences an electric field $\sim v_b \delta B_W$, which accelerates the electron in the transverse direction. Clearly, the higher the velocity along the ambient magnetic field, the more effective the scattering. In the wave frame, the kinetic energy of the electron is conserved, which implies that in the observer's frame, the electron energy is approximately conserved (because the Alfvén speed is low in comparison to the beam speed), but its pitch angle will change. The unperturbed distribution function is constructed on the basis of two constants of motion, $mv^2/2$, the total energy, and the canonical angular momentum, $p_\perp - eA_\perp \gamma/c$, where $A_\perp$ denotes the vector potential of the Alfvén wave field and γ is the relativistic factor.

We introduce the normalized momentum $\boldsymbol{u} = \boldsymbol{p}/mc$. The model distribution function of the beam electrons $F_b(u_\parallel, u_\perp)$, where $u_\parallel$ and $u_\perp$ are momentum components parallel and perpendicular to the ambient magnetic field, respectively, is given by

$$F_b(u_\parallel, u_\perp) \sim \exp\left[-\frac{(u - u_0)^2}{\Delta^2} - \frac{(u_\perp - u_s)^2}{\alpha^2} \right], \quad (3)$$

where $u = (u_\parallel^2 + u_\perp^2)^{1/2}$, Δ and α denote the momentum dispersions in the radial and perpendicular directions, respectively, u_0^2 represents the average normalized beam kinetic energy, and u_s is a constant. Hereafter, we assume that Δ is small in comparison to the beam momentum u_0. We also assume that $\alpha > \Delta$. To facilitate our discussion, we henceforth rewrite equation (3) as

$$F_b(u_\parallel, u_\perp) = D \exp\left[-\frac{(u - u_0)^2}{\Delta^2} - \frac{(\sqrt{1-\mu^2} - \nu)^2}{\beta^2} \right], \quad (4)$$

where we have defined that $\mu = u_\parallel/u \approx u_\parallel/u_0$, $\nu \equiv u_s/u_0$, $\beta \equiv \alpha/u_0$, and

$$\frac{1}{D} = 2\pi\Delta^3 \left[\frac{u_0}{\Delta} e^{-u_0^2/\Delta^2} + \frac{\sqrt{\pi}}{2}\left(1 + \frac{2u_0^2}{\Delta^2}\right)\left(1 + \mathrm{erf}\frac{u_0}{\Delta}\right) \right]$$
$$\times \int_0^1 d\mu \exp\left[-\frac{(\sqrt{1-\mu^2} - \nu)^2}{\beta^2} \right]. \quad (5)$$

Besides the effect of pitch-angle scattering by Alfvén waves, the magnetic field gradient might also affect the beam distribution function. We argue that in the presence of excited waves with frequencies close to the gyrofrequency, the electron magnetic moment is not conserved. Even if the magnetic moment can be approximately conserved, we expect that its effect on the distribution function is less important than that of the pitch-angle scattering, since the spatial scale length of the pitch-angle scattering process is

far shorter than the scale height of the ambient magnetic field.

The distribution function described by equation (3) can lead to a maser instability. Basically, the nature of the instability is qualitatively similar to that of the usual maser instability driven by a loss-cone distribution (see reviews by Melrose 1986, p. 194; Benz 1993, and references therein), or to a partial-shell distribution (Yoon, Weatherwax, & Rosenberg 1998). We are interested in fast electromagnetic waves with two independent polarizations, i.e., the O (ordinary) and X (extraordinary) modes. The dispersion relation for these waves can be written as

$$N_\sigma^2 = \epsilon_\sigma \quad (\sigma = X, \ O) \ ,$$

$$\epsilon_X = 1 - \frac{f_p^2}{f(f + \tau f_g)} \ , \quad \epsilon_O = 1 - \frac{\tau f_p^2}{f(\tau f - f_g \cos \theta)} \ ,$$

$$\tau = \left(s + \sqrt{\cos^2 \theta + s^2} \right) \frac{f_p^2 - f^2}{|f_p^2 - f^2|} \ , \quad s = \frac{f f_g \sin^2 \theta}{2|f_p^2 - f^2|} \ , \quad (6)$$

where θ is the wave phase angle defined with respect to the ambient magnetic field. The temporal cyclotron growth/damping rate, which includes damping by the background electrons, is given by

$$f_i^\sigma = \frac{\pi f_p^2}{2} \frac{1}{f} \frac{1}{(1 + T_\sigma^2) R_\sigma} \sum_{n=-\infty}^{\infty} \int d^3 \boldsymbol{u} \, (1 - \mu^2)$$

$$\times \, \delta \left(\sqrt{1 + u^2} - \frac{n f_g}{f} - N_\sigma u \mu \cos \theta \right)$$

$$\times \left\{ \frac{f}{f_g} [K_\sigma \sin \theta + T_\sigma (\cos \theta - N_\sigma u \mu)] \frac{J_n(b_\sigma)}{b_\sigma} \right.$$

$$\left. + J_n'(b_\sigma) \right\}^2 \left[u \frac{\partial}{\partial u} + (N_\sigma u \cos \theta - \mu) \frac{\partial}{\partial \mu} \right] F_e(u, \ \mu) \ , \quad (7)$$

where

$$R_X = 1 - \frac{\tau f_p^2 f_g (1 + U)}{2f(f + \tau f_g)^2} \ , \quad R_O = 1 + \frac{\tau f_p^2 f_g \cos^2 \theta (1 - U)}{2f(\tau f - f_g \cos^2 \theta)^2} \ ,$$

$$U = \frac{\tau^2 - \cos^2 \theta f^2 + f_p^2}{\tau^2 + \cos^2 \theta f^2 - f_p^2} \ , \quad b_\sigma = \frac{f}{f_g} N_\sigma \sin \theta u (1 - \mu^2)^{1/2} \ ,$$

$$T_X = -\frac{\cos \theta}{\tau} \ , \quad T_O = \frac{\tau}{\cos \theta} \ , \quad K_X = \frac{f_p^2}{f^2 - f_p^2} \frac{f_g \sin \theta}{f + \tau f_g} \ ,$$

$$K_O = \frac{f_p^2}{f^2 - f_p^2} \frac{\tau f_g \sin \theta}{\tau f - f_g \cos^2 \theta} \ . \quad (8)$$

Here $J_n(b)$ is the Bessel function of the first kind, with the prime denoting the derivative with respect to the argument.

The temporal growth rate for the X and O modes, respectively, is numerically computed on the basis of the above formula. As a sample case, let us choose $u_0 = 0.5$, $\Delta = 0.1 u_0$, $\beta = 0.3$, and $\nu = 0.2$, for which the bulk average velocity is roughly $0.4c$. In Figure 3 (top) we show the maximum temporal growth rates of the X and O modes as functions of the parameter f_p/f_g. Figure 3 (bottom) displays contour plots of the growth rates versus normalized wave frequency and the wave-normal directions. Hereafter, we introduce the shorthand notations X1 and O1 to denote X-
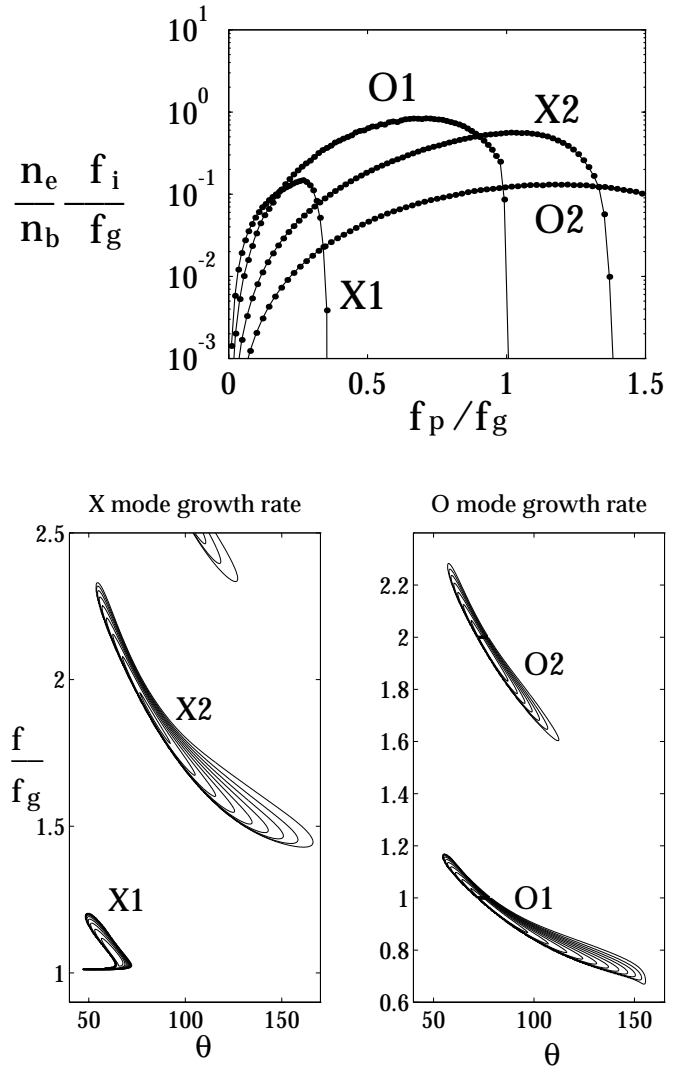
Fig. 3.—Top: Normalized maximum growth rates vs. the ratio f_p/f_g. Bottom: Contour plots of the growth rate as functions of frequency and wave normal angle θ, for $f_p/f_g = 0.1$. In obtaining these numerical results, the beam velocity is taken to be $0.4c$. We also choose $\Delta = 0.1 u_0$ and $\beta = 0.3$. X and O denote the X mode and O mode, respectively. Suffixes 1 and 2 indicate the fundamental and second harmonic components, respectively.

and O-mode waves near the gyrofrequency, while X2 and O2 are waves near the second harmonic, 2Ω. It is seen that all excited waves have nearly perpendicular propagations except X1.

The temporal growth rate f_i in a finite source region may not necessarily be the best quantity to characterize the property of a given mode, owing to convective effects. Thus, we also calculate the spatial amplification rate, denoted by Γ,

$$\Gamma = \frac{f_i}{v_g} \ ,$$

where v_g is the group velocity. In Figure 4 we present the maximum value of Γ versus the parameter f_p/f_g.

The essential findings of the instability analysis can be summed up as follows:

1. The bandwidth of the excited F or H waves is finite but narrow.

$$\frac{n_e}{n_b} \frac{c\,\Gamma_{max}}{f_g}$$
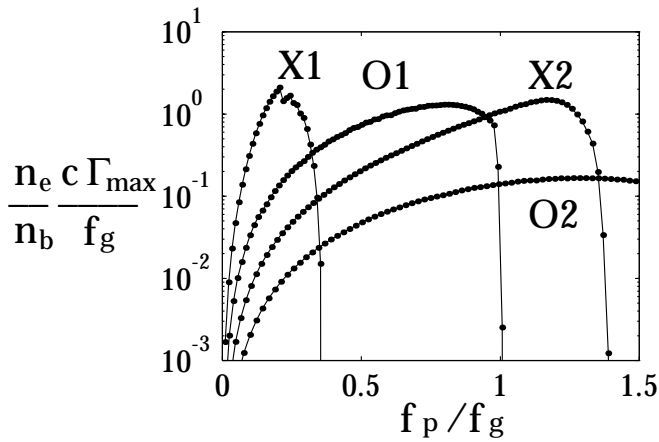
FIG. 4.—Normalized spatial amplification rate vs. the ratio f_p/f_g for the case shown in Fig. 3.

2. The amplification is suppressed if the ratio f_p/f_g is too small, which implies that the instability will not be operative at very low altitudes.

3. In our model, the region that covers the primary frequency range of interest is characterized by $0.1 < f_p/f_g < 0.3$, as shown in Figure 2. In this region, the X1 mode prevails over O1, while the X2 mode has a higher growth rate than O2. Here we note that although the X1 spatial growth rate is higher than that of X2, the effective distance for amplification of an X2 mode is much longer, since the detuning effect on the resonance condition by the magnetic field gradient is more significant on the X1 waves. This is because X1 modes initially propagate with oblique phase angles, while X2 waves propagate in nearly perpendicular directions.

4. As shown in Figure 3 (*bottom*), X2 and O1 waves with a negative wavevector $k_\parallel$ parallel to the ambient magnetic field, or equivalently, with $\theta > 180°$, can be excited as well. These waves are significant in a plausible scenario for type V bursts.

5. Growth rates of both O3 and X3 are small and negligible in comparison to X2.

To summarize, a preliminary conclusion is that in a strongly magnetized plasma, a beam of fast electrons can lead to direct amplification of electromagnetic waves with frequencies close to the fundamental and second harmonic of the electron gyrofrequency, provided that the ratio f_p/f_g is sufficiently small, as shown in Figure 3 (*top*). We suggest that type III bursts are produced by a cyclotron-maser instability driven by electrons streaming through a density-depleted duct in which the ratio of the local plasma frequency to the electron gyrofrequency, f_p/f_g, is sufficiently low (see Fig. 2). In this model, the observed F-H pair emission corresponds to electromagnetic waves with frequencies close to the local electron gyrofrequency (f_g) and its second harmonic ($2f_g$), instead of the plasma frequency (f_p) and its harmonic ($2f_p$). Since the excited waves are produced inside a low-density duct, the waves are initially confined to the duct, until they escape from the "apparent source" at higher altitudes where the wave frequency matches the local cutoff frequency. In this way, the observed dynamic spectrum is affected by both the exterior plasma frequency and the gyrofrequency in the actual source region.

If an observer detects the emitted waves at a fixed frequency, then the observed waves would be seen as having two consecutive bursts. The reason is because the streaming electrons first excite waves at a certain altitude where the local electron gyrofrequency is close to the wave frequency. Then, as the beam electrons move up the field, they will excite waves at a second site at a higher altitude, where the wave frequency is close to twice the local gyrofrequency. In this sense, the notions proposed in Rosenberg (1975) and Daigne (1975b) are compatible with our model.

The observation of the F component is subject to two conditions. First, the F waves can be excited only if the electron density inside the duct is sufficiently low (Fig. 3 [*top*]). In contrast, the H waves are excited over a wider range of f_p/f_g. Second, the F waves are much more directive than the H waves, a point to be discussed later. Consequently, the F waves are expected to be less observable.

The present model does not rule out the possibility that the plasma emission mechanism may also be operative in the duct (Duncan 1979; Robinson & Cairns 1998a). However, the available theories for the plasma emission mechanism cannot be immediately applied to the physical regions modeled in our theory, since these theories are valid for regions where the ambient magnetic field is weak. A strong magnetic field not only affects the physical kinetics but also modifies the nonlinear wave-wave and wave-particle processes. The emission process in the present model is by direct amplification, which is in general more efficient than indirect conversion processes. Furthermore, with the severe density depletion considered in our model, the emitted wave frequency that results from the plasma emission process would be too low to be of interest anyway. Study of the nonlinear saturation of the excited waves is beyond the scope of the present discussion.

Finally, the present model does not include the effects of density irregularities that are considered by others (Duncan 1979; Robinson & Cairns 1998a). These authors find that the density turbulence can cause electromagnetic rays with frequencies near the plasma frequency, i.e., can cause the F component (under the assumption that these waves are excited by the plasma emission mechanism) to be randomly reflected and trapped, thereby leading to a significant time delay in comparison to the wave with frequency near twice the plasma frequency (H component), which is unaffected by the density irregularity. In the future, it is desirable to consider such an effect in the context of our model. However, since the primary constraint on the wave propagation in our model comes from the severely density-depleted duct that acts as a waveguide for the electromagnetic rays, we believe that small-amplitude density fluctuations will not affect the main conclusion of our work.

4. DISCUSSION

In the preceding sections, we have presented a brief description of the proposed scenario. In the following, we discuss consequences of such an emission model. To facilitate our discussion, we first present Figure 5, in which we plot the interior and exterior plasma frequency, the gyrofrequency, and its second harmonic. We also plot the X-mode cutoff frequency outside the duct that determines the altitude at which the waves exit the duct. All these quantities are computed on the basis of the density and magnetic field models described in § 2.
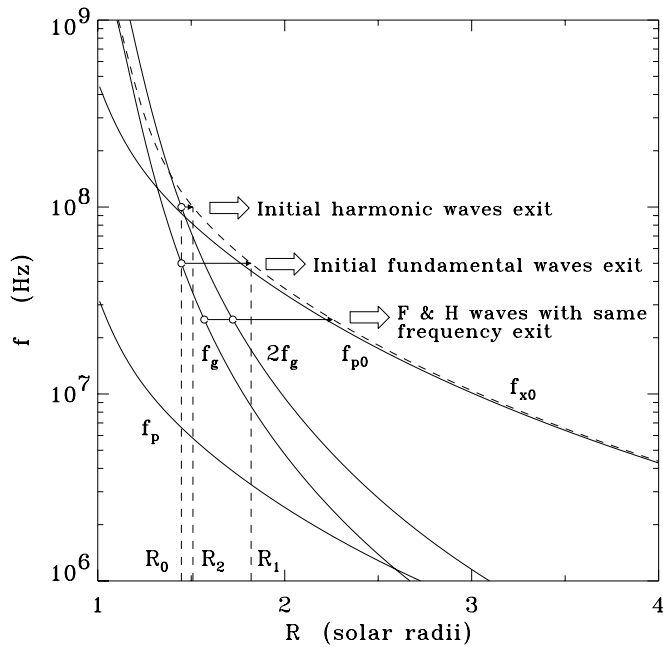
FIG. 5.—Interior and exterior plasma frequency, the X-mode cutoff frequency, and the gyrofrequency, as well as its second harmonic, plotted vs. the altitude R ($R = 1$ at the photosphere). Here, R_0 marks the initial position where the type III emission commences. The plot is based on the density models and magnetic field model discussed in § 2.

4.1. *Wave Propagation in a Duct*

To estimate the "propagation" speed of a wave inside the duct is a desirable task. Since the amplified waves initially propagate in directions either nearly perpendicular (X2) or oblique (X1) to the ambient magnetic field, it is anticipated that they must undergo multiple reflections off the density wall before they escape to free space.

Making use of the present density and magnetic field models, we can estimate the radial distance L each wave must traverse before exiting. Since waves with different frequencies are generated at different altitudes, we can consider the distance L as a function of the wave frequency, as shown in Figure 6 (*top*). The quantity L can be viewed as a measure of the projected duct length in the radial direction. As frequency decreases with increasing altitude, the corresponding distance L increases. In Figure 6 (*top*) we consider the situation in which both F- and H-component waves are excited inside the duct and assume that emission starts at the altitude where the H-mode frequency is equal to the exterior X-mode cutoff frequency.

In order to estimate the propagation velocity, we consider a straight duct. Its cross section is considered to vary with altitude, which can be determined from the conservation of magnetic field flux. In the calculation, both the F and H waves are assumed to satisfy the X-mode dispersion relation, and we make use of Snell's law. We assume that the transverse profile of the interior electron density at a given altitude is nearly constant. We also consider that the initial wave normal direction for X2 is close to $90°$, whereas for X1, the angle is $\leq 60°$ (Fig. 3 [*bottom*]).

The computation was carried out with several values of effective duct radius at the starting altitude. We then computed the propagation velocity along the duct. It turns out that numerical results are insensitive to the duct radius. On
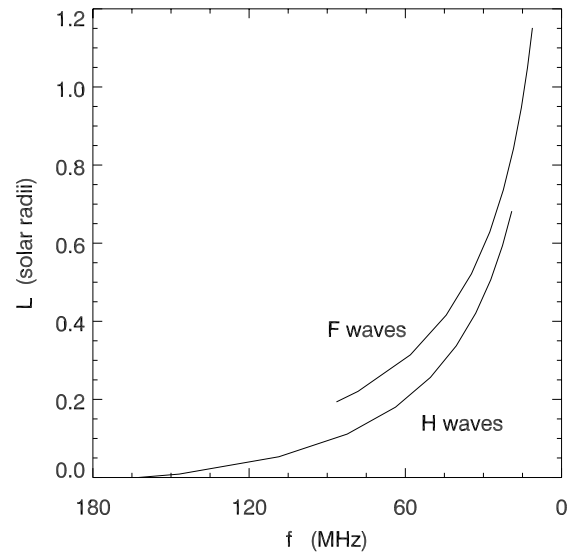
FIG. 6a
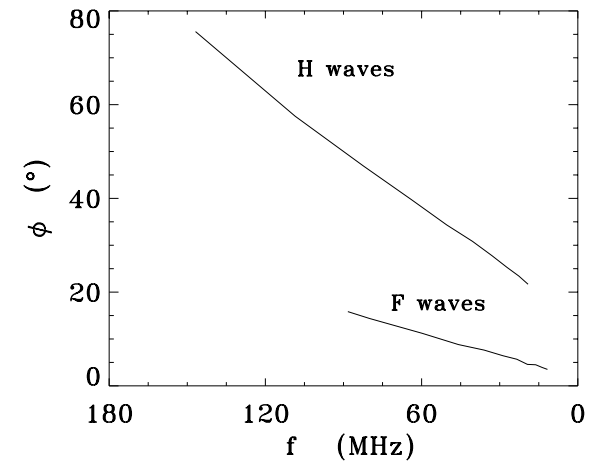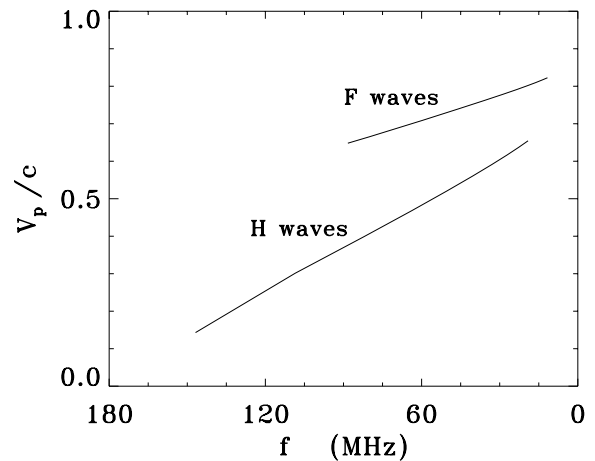
FIG. 6b

FIG. 6.—(a) Radial distance L vs. frequency of the emitted waves calculated from Fig. 5. At a given frequency, the F wave has a longer distance to propagate than the H wave before exiting. (b) *Top*: Estimates of propagation speeds vs. frequency of the emitted wave. These estimates are obtained by considering straight ducts pointing in the radial direction. They only represent the upper bounds of the propagation speeds. *Bottom*: Angle of propagation ϕ at the exit vs. frequency of the F wave and the H wave. The quantity ϕ is defined to be the angle between the ray path and the ambient magnetic field, which is parallel to the duct axis.

the basis of the same consideration in Figure 6a, the propagation speed v_p is plotted in Figure 6b (*top*) as a function of the emitted wave frequency. For convenience, v_p is spatially averaged over the distance traversed by each wave before exiting. In Figure 6b (*bottom*) we plot the angle between the ray path of a wave and the axis of the duct, ϕ, versus wave frequency. This result has an important implication on the directivity. We return to this point later in § 4.4.

Since a realistic duct should lie along the ambient magnetic field lines in the corona, which is neither straight nor necessarily in the radial direction, the actual length of the duct is in general much longer than L. Moreover, the curvature of a bending duct can also seriously affect the propagation speed. In view of these difficulties, we note that a general and rigorous discussion is evidently not feasible. Thus, readers should bear in mind that the results displayed in Figure 6b (*top*) represent the upper bounds of the propagation speeds of F waves and H waves. However, two qualitative conclusions may be pertinent: First, F waves have a higher propagation speed than H waves. Second, as shown in Figure 6b (*bottom*), ray paths of F waves are nearly parallel to the ambient field when they exit from the duct.

Owing to the different duct lengths and propagation speeds associated with the F waves and H waves, there are important consequences. Among them is the initial time delay between the F waves and H waves that is generally observed (e.g., Suzuki & Dulk 1985). Conventional theories suggest that this time delay might be due to the effect of the group delay of the F waves, which have frequencies close to the local plasma frequency (e.g., Stewart 1974b; Robinson & Cairns 1998a).

In the following, we offer an alternative explanation. From Figure 5 one can see that H waves always exit at a lower altitude than F waves before they escape. If F and H waves are initially produced at R_0, the F component exits at R_1, while the H wave exits at R_2. As a result, it is expected that the F component trails the H component with a time delay. This time delay should occur for all subsequently emitted waves. To quantify the actual time delay is not so straightforward, however. For a qualitative estimate, we can either assume an effective duct length longer than what is shown in Figure 6a or assume an effective propagation speed projected onto the radial direction. The estimated initial time delay turns out to be on the order of a few seconds. Finally, we note that the F waves in our model lie close to the X-mode cutoff frequency. However, numerical tests find that the effect of group delay does not lead to a significant time delay.

4.2. H/F Frequency Ratio

It is well known that the observed H/F frequency ratio of type III bursts at a given time in the dynamic spectrum is usually below 2. The average value is roughly $\sim$1.8 (Wild, Murray, & Rowe 1954; Stewart 1974b). The explanation based on the present model is as follows: Two factors affect the H/F frequency ratio. First, X1 waves have a maximum amplification rate above but near the cutoff frequency, which in the strong field region is $f_g(1 + f_p^2/f_g^2)$, while X2 waves have a maximum amplification rate near $2f_g/(1 + u_0^2)^{1/2}$. Thus, we expect that the H/F frequency ratio should be about $2[1/(1 + u_0^2)^{1/2} - f_p^2/f_g^2]$. Second, the time delay of F-mode over H-mode waves, which occurs over a broad range of frequencies, may further reduce the

H/F ratio observed at a given time. In theories based on the plasma emission process, it is often suggested that the H/F frequency ratio is dictated by the scattering of the F waves by density fluctuations (Robinson & Cairns 1998a).

A couple of remarks are necessary at this point. First, it is important to reiterate that in the above discussion, the quantity f_p^2/f_g^2 is specified in the source region rather than at the exit region. One should remember that it is attributed to the consideration that X1 waves have frequencies close to the cutoff frequency $f \approx f_g(1 + f_p^2/f_g^2)$ in the source region. Second, observations discussed in the literature seem to suggest that the beam velocities range from $0.2c$ to $0.6c$ and the H/F frequency ratio on average is about 1.8 ± 0.14 (e.g., Suzuki & Dulk 1985). According to our model (see Figs. 2 and 5), the ratio f_p/f_g varies with altitude, and so does the H/F frequency ratio. For instance, in low-altitude regions, where $f_p/f_g \approx 0.1$–0.2, the H/F frequency ratio is estimated to be 1.67 for $u_0 = 0.6$ and 1.88 for $u_0 = 0.2$. At higher altitudes, where $f_p/f_g \approx 0.3$, the same is estimated to be 1.53 for $u_0 = 0.6$ and 1.78 for $u_0 = 0.2$.

4.3. Dynamic Spectrum

A sample numerically calculated dynamic spectrum is plotted in Figure 7 (*left*). The calculation is carried out with the following choice of parameters: The beam velocity projected onto the radial direction is considered to be $0.1c$, while an effective propagation speed is chosen to be 0.4 times that shown in Figure 6b for F waves and H waves; we assume that type III emission initiates at $t = 0$, and F waves have starting frequencies around 90 MHz. In this case, we find an initial time delay of about 1.5 s.

At this point, it would be appropriate to explain why we chose a low beam velocity $0.1c$ to calculate the dynamic spectrum, while for the instability calculation, we chose $u_0 = 0.5$ (which corresponds to an average parallel beam speed of $\sim 0.4c$). The latter choice of $u_0 = 0.5$ was made with respect to the observations that suggest an average beam speed of roughly $0.2c$–$0.6c$. However, the dynamic spectrum calculation is based on a one-
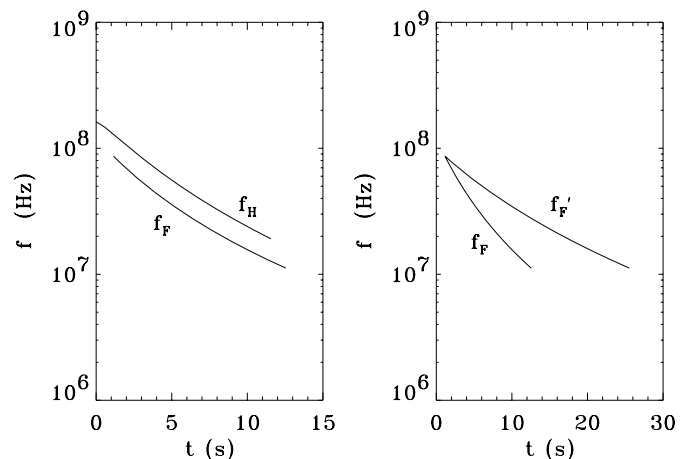
Fig. 7.—*Left*: Calculated dynamic spectrum in time. In obtaining it, we have considered a number of assumptions, as discussed in the text. *Right*: For the purpose of comparison, a dynamic spectrum based on the plasma emission hypothesis, denoted by f_F'. In obtaining it, we have considered similar conditions to those used for obtaining the left panel. It is seen that the present model gives rise to a higher rate of frequency drift.

dimensional model in which all quantities depend only on the radial distance R. Since in general the flux tubes in which the radio source is embedded are not only three-dimensional but also curved, physically we ought to adopt an "effective" beam velocity rather than that used in the discussion of the instability. Conceptually, this effective beam velocity can be considered as the beam velocity projected onto the radial direction. In the present discussion, we postulate that the effective beam velocity might be taken to be in the range $0.1c$–$0.3c$. The choice of $0.1c$ demonstrates that even if such a low value is used, the present model still leads to a fairly high frequency drift.

Two remarks are pertinent. First, according to the present model, the dynamic spectrum yields a higher rate of frequency drift than that in the case in which the radiation is generated via the plasma emission process. Second, in the present model, a wave at the apparent source has a frequency higher than the local plasma frequency because it must have a frequency slightly above the local X-mode cutoff frequency rather than the local plasma frequency, as indicated in Figure 5.

This finding has some significant implications. In the past, the beam speed was estimated on the basis of the assumption that the spectrum is dictated by the density profile in the corona. Combined with a density model, the beam speed can then be computed from the observed frequency drift. If our scenario is true, then the usual interpretation of the observed dynamic spectrum will lead to an overestimation of the beam velocity. This point seems to be consistent with the discussions by Dulk (2000) and Dulk, Steinberg, & Hoang (1987), who argue that the actual beam velocity may be much lower than that previously suggested in the literature. On the other hand, the proposed scenario can be used as an indirect means to estimate the coronal magnetic field. In Figure 7 (right) we have generated a dynamic spectrum based on the plasma-emission model with the same beam velocity. For simplicity, we only present the F component (f'_F). In the same figure, we also show the F component depicted in Figure 7 left) for comparison (f_F).

4.4. Polarization and Directivity

According to Figure 4, at the fundamental gyrofrequency f_g, the X1 dominates over O1 over the range $0.1 \leq f_p/f_g \leq 0.3$, while at the harmonic $2f_g$, X2 dominates over O2. The range of f_p/f_g values greater than ~ 0.3 is not of practical interest, since the altitude range characterized by $f_p/f_g > 0.3$ corresponds to emission frequencies below the observable range from ground-based facilities. From this, we claim that both F and H components should be X-mode polarized.

However, this conclusion is based on the present density model. Different models with less severe density depletion may correspond to higher f_p/f_g. For this reason, it is important to consider the further implications of Figure 4. For instance, according to Figure 4, the O1 mode would be the only fundamental emission if $0.4 \leq f_p/f_g \leq 1$, while X2 would still prevail over O2. Similarly, if $f_p/f_g > 1$, no fundamental emission is possible, and only the X-mode polarized H component is expected.

Here we note that although Figure 4 was obtained for a specific set of physical parameters, dependence of the results on parameters other than f_p/f_g, such as average beam speed, momentum spread associated with the beam electrons, etc., appears to be less critical. Therefore, we believe that the spatial growth properties of various modes are well represented by Figure 4 in an overall sense. We also note that linear stability analysis only describes the initial conditions for wave growth. To complete the discussion, one must evaluate the saturation wave amplitudes.

A consensus reached on the basis of available observations appears to be that in the event of F-H pair emission, the sense of polarization for the F component is the same as that of the H component (Dulk & Suzuki 1980; Suzuki & Dulk 1985). However, our theory implies that an O-mode polarized F component and an X-mode polarized H component should be possible when the source region is characterized by $0.4 \leq f_p/f_g \leq 1$. The issue is, then, why such cases are not observed.

Our tentative explanation is based on the difference between the wave energy density associated with the O mode versus the X mode. We expect the O-mode wave intensity to be much lower than that of X1 waves, because the spontaneous emissivity of O1 waves is generally much lower than that of X1 waves. To see this, let us denote the wave energy by W and the spontaneous emissivity by S. Then the equation for wave energy density along the ray path can be written as

$$\frac{dW}{dt} = 2f_i W + S \, , \tag{9}$$

where ω_i is the temporal growth rate. The first term on the right-hand side describes an induced emission process, while the second term represents spontaneous emission. In general, both f_i and S are time-varying quantities. Equation (9) in quasi-linear approximation is discussed by Wu (1968) and Melrose (1980), for instance.

Here we remark that the spontaneous emissivity S is different from that computed for thermal equilibrium, for which S would exactly balance $-2|f_i|W$. In the present case, few thermal electrons with energies 100–200 eV can resonate with the unstable waves that are excited by the beam electrons with bulk kinetic energy ~ 100 keV. In short, we can simply ignore the thermal electrons in equation (9).

For the sake of discussion, however, let us treat f_i and S as quasi-stationary. Then equation (9) yields

$$W(t) \approx W(0)e^{2f_i t} + \frac{S}{f_i}(e^{2f_i t} - 1) \, , \tag{10}$$

which implies that if the initial seed perturbation is small, $W(0) \sim 0$, then the leading term for $W(t)$ is

$$W(t) \approx \frac{S e^{2f_i t}}{f_i} \, . \tag{11}$$

To compute the quantity S, let us simplify the situation by considering waves propagating in nearly perpendicular directions and pay attention to the case $f \approx f_g$. If we denote S_O and S_X to be the O-mode and X-mode emissivity, respectively, then one can obtain

$$S_O \sim \int d^3 \boldsymbol{u} \, u^2 \mu^2 J_1^2(b_O)$$
$$\times \delta \left(\sqrt{1 + u^2} - \frac{f_g}{f} - N_O u \mu \cos \theta \right) F_e(u, \, \mu) \, , \tag{12}$$

$$S_X \sim \int d^3\boldsymbol{u}\, u^2(1-\mu^2)J_0^2(b_X)$$

$$\times\, \delta\left(\sqrt{1+u^2} - \frac{f_g}{f} - N_X u\mu\cos\theta\right)F_e(u,\ \mu)\ , \quad (13)$$

where F is the distribution function of the emitting electrons. One can further simplify the situation by noting that $J_1^2 \ll J_0^2 \approx 1$ for b_O, $b_X \ll 1$. Thus, we see that $S_O \ll S_X$; hence, the O-mode intensity is expected to be generally much lower than that of the X mode.

Past discussions of type III polarization in the literature seem to favor the O mode, but there are uncertainties. All the discussions are based on some kind of inference or hypothesis. The difficulty stems from the fact that existing methods of observation can only measure the sense of polarization of the radiation, rather than the actual wave mode (see the recent discussion along this line by Wu, Yoon, & Li 2000b).

Another important issue concerns the directivity of F and H waves. In this regard, Figure 6b (*bottom*) is relevant, on the basis of which we had concluded that the F component has much higher directivity than the H component. This is to be expected on an intuitive ground, since the F waves initially propagate in the oblique directions, while H waves are excited with wavevectors primarily along perpendicular directions. Moreover, F waves must propagate much longer along the duct and emerge from the end of the duct much later when compared to the H component generated at the same source. These seem to be in good agreement with observations (Caroubalos & Steinberg 1974; Caroubalos, Poquerusse, & Steinberg 1974; Dulk & Suzuki 1980; Suzuki & Dulk 1985) that conclude that F components of F-H pairs are generally more directive than H components. As a result, H components should be more observable than F components. Perhaps this could contribute to why F-H pairs are less observed than single-banded type III emissions. In contrast to the present model, the standard plasma emission mechanism tends to favor H components as being more directive, since F-component waves are more susceptible to scattering by density fluctuations.

5. COMMENTS ON THE RELATION BETWEEN TYPE III AND TYPE V EMISSIONS

Although solar radio bursts of various types show different spectral characteristics, some of them may actually share the same underlying emission process. We propose that type III and V emissions are such an example.

Spectral type V emission generally appears as a broadband diffuse afterglow that immediately follows a type III emission (Wild, Sheridan, & Trent 1959b; Wild, Sheridan, & Neyland 1959a; Weiss & Stewart 1965; Labrum & Duncan 1974; Robinson 1977, 1978; Dulk & Suzuki 1980), which implies that type V radio emission is closely associated with type III bursts. It is therefore possible that the two phenomena may result from the same emission model. In the following, we offer a preliminary discussion.

We advocate that the maser instability responsible for type III bursts may also result in type V emission. The outstanding point is that type III emission is due to X-mode waves propagating in an upward direction (parallel to the beam velocity, i.e., waves with $k_\parallel > 0$), whereas type V emission is due to O-mode waves propagating in a downward direction (antiparallel to the beam velocity, with $k_\parallel < 0$). For type V emission, downward O1 waves are most relevant, although in principle, O2 and X2 waves with $k_\parallel < 0$ can also be excited. Let us explain.

Our discussion assumes at the outset that in the source regions, the parameter ω_p/Ω is sufficiently small that the instability condition is met. We note that the O2-mode growth rate is at least an order of magnitude smaller than that of O1 waves; hence, O2 waves can be ignored. Although the X2 growth rate may be comparable to that of O1, downward X2 waves would be reflected immediately because the X-mode cutoff frequency is between Ω and 2Ω. Thus, only O1 waves can propagate to a low-altitude region, where they will be reflected when the local plasma frequency is equal to the wave frequency. The reflected O-mode will then propagate back upward and escape at high altitudes where the exterior plasma frequency is equal to the wave frequency. We suggest that these waves are observed as type V waves. Thus, the polarization of type V emission is in the sense of the O mode, while type III bursts are X-mode polarized. The opposite polarizations of the two types of emissions seem to be in agreement with observations (Dulk, Suzuki, & Gary 1980; Suzuki & Dulk 1985).

Let us consider downward O-mode waves with frequencies around 30 MHz, for instance. The radial distance between the point of excitation and the reflection point, which can be visually estimated from Figure 5, is roughly $0.5\,R_\odot$. On the other hand, for downward waves with nearly perpendicular propagation, the effective propagation speed along the duct is expected to be very low. If we postulate the effective propagation speed to be $0.1c$ or lower, then we estimate that the time required between excitation and exit from the duct is at least a few tens of seconds.

In regions where the ratio f_p/f_g is small, the X- and O-mode cutoff frequencies are significantly different. This point implies that type III and V bursts would exit at different altitudes and points. Consequently, their apparent source positions are expected to be different. This may account for the observed position shift reported in the literature.

In our model, the density-depleted duct extends to the upper chromosphere. We suppose that the interior electron density (and thus the local plasma frequency) is highest at the lower end of the duct. This maximum plasma frequency is important to the discussion of the type V emission because those downward propagating O-mode waves with frequencies above it would propagate into the chromosphere and be absorbed because of collisional damping. This may explain why type V emission usually occurs with low frequencies, say several tens of megahertz, and rarely happens above 100 MHz. In the present discussion, we arbitrarily choose 30 MHz to be the maximum interior plasma frequency, and we have modeled the interior electron density accordingly. However, any choice of frequency between 10 and 100 MHz would be acceptable.

That the cyclotron-maser model lends itself to a unified model of type III and V bursts is a strength of the present scenario. To the best of our knowledge, no such generalization is available within the context of the plasma-emission model. A more detailed quantitative analysis of type V emission within the context of the present model will be reported in a forthcoming article.

6. CONCLUDING REMARKS

To summarize, we have proposed a model to explain type III radio bursts in the solar corona near active regions, where the ambient magnetic field is supposed to be strong. In contrast, conventional models that ignore the effects of the ambient magnetic field may be appropriate for interplanetary type III emission. Our model relies on the existence of underdense ducts in the corona (Duncan 1979), and the underlying radiation emission mechanism is a beam-maser instability that leads to direct amplification of radiation. It is assumed that the electron density inside the duct is significantly lower than the outside. In the proposed model, we find that the emission of the fundamental component requires $0.1 \leq f_p/f_g \leq 0.4$ in the source region. Thus, in the present discussion we have considered an arbitrary depletion factor of approximately 10^2 near the chromosphere. The assumed depletion factor may be lower if a stronger magnetic field model is used.

One of the consequences of our model is that the observed frequency drift reflects the decreasing magnetic field strength along the path of the streaming electrons, rather than the density, as assumed in conventional theories. The frequency of an emitted wave is determined by the local gyrofrequency at the "true" source altitude where the mode is generated. The local gyrofrequency at low altitudes can be much higher than the local plasma frequency. However, in the "apparent" source region where the waves escape, the X-mode cutoff frequency, which is higher than the local exterior plasma frequency, dictates the exit point of the radiation from the duct.

The discussion presented in this paper is preliminary. More research is needed to fully understand many related issues. Finally, some comments on the recent work by Wu, Li, & Yoon (2000a) and Wu et al. (2000b) are necessary. One of the shortcomings pertains to the fact that the model is rather sensitive to the geometrical configuration of the magnetic field and density gradient in the source region. It is also implicitly required that the plasma be quiescent and that small-scale density or magnetic irregularities be absent, so that the dispersion relation of the gyroharmonics can be meaningful. These requirements and assumptions may not be satisfied in the real coronal situation.

REFERENCES

Aschwanden, M. J., & Benz, A. O. 1997, ApJ, 480, 825
Benz, A. O. 1993, Plasma Astrophysics (Dordrecht: Kluwer)
Bougeret, J. L., Caroubalous, C., Mercier, C., & Pick, M. 1970, A&A, 6, 406
Bougeret, J. L., & Steinberg, J. L. 1977, A&A, 61, 777
Cairns, I. H. 1987a, J. Plasma Phys., 38, 169
———. 1987b, J. Plasma Phys., 38, 179
———. 1987c, J. Plasma Phys., 38, 199
Caroubalos, C., Poquerusse, M., & Steinberg, J. L. 1974, A&A, 32, 255
Caroubalos, C., & Steinberg, J. L. 1974, A&A, 32, 245
Daigne, G. 1975a, A&A, 38, 141
———. 1975b, A&A, 42, 71
Dulk, G. A. 1985, in Solar Radiophysics, ed. D. J. McLean & N. R. Labrum (New York: Cambridge Univ. Press), 19
———. 2000, in Radio Astronomy at Long Wavelengths, ed. R. G. Stone, K. W. Weiler, M. L. Goldstein, & J.-L. Bougeret (Washington, DC: AGU), 115
Dulk, G. A., & McLean, D. J. 1978, Sol. Phys., 57, 279
Dulk, G. A., Steinberg, J.-L., & Hoang, S. 1987, A&A, 173, 366
Dulk, G. A., & Suzuki, S. 1980, A&A, 88, 203
Dulk, G. A., Suzuki, S., & Gary, D. E. 1980, A&A, 88, 218
Duncan, R. A. 1979, Sol. Phys., 63, 389
Ginzburg, V. L., & Zheleznyakov, V. V. 1958, Soviet Astron.—AJ, 2, 653
Goldman, M. V. 1983, Sol. Phys., 89, 403
Kai, K., Melrose, D. B., & Suzuki, S. 1985, in Solar Radiophysics, ed. D. J. McLean & N. R. Labrum (New York: Cambridge Univ. Press), 415
Labrum, N. R., & Duncan, R. A. 1974, in IAU Symp. 57, Coronal Disturbances, ed. G. Newkirk, Jr. (Dordrecht: Reidel), 235
Leblanc, Y. 1973, Astrophys. Lett., 14, 41
McLean, D. J. 1971, Australian J. Phys., 24, 201
———. 1985, in Solar Radiophysics, ed. D. J. McLean & N. R. Labrum (New York: Cambridge Univ. Press), 37
Melrose, D. B. 1980, Plasma Astrophysics (New York: Gordon & Breach), chap. 5
———. 1985, in Solar Radiophysics, ed. D. J. McLean & N. R. Labrum (New York: Cambridge Univ. Press), 177
———. 1986, Instabilities in Space and Laboratory Plasmas (New York: Cambridge Univ. Press)
Mercier, C., & Rosenberg, H. 1974, Sol. Phys., 39, 193
Newkirk, G., Jr. 1967, ARA&A, 5, 213
———. 1971, in IAU Symp. 43, Solar Magnetic Fields, ed. R. Howard (Dordrecht: Reidel), 547
Poquerusse, M., & McIntosh, P. S. 1995, Sol. Phys., 159, 301
Riddle, A. C. 1972, Proc. Astron. Soc. Australia, 2, 98
———. 1974, Sol. Phys., 35, 153

Robinson, P. A., & Benz, O. A. 2000, Sol. Phys., 194, 345
Robinson, P. A., & Cairns, I. H. 1994, Sol. Phys., 154, 335
———. 1998a, Sol. Phys., 181, 363
———. 1998b, Sol. Phys., 181, 395
———. 1998c, Sol. Phys., 181, 429
Robinson, P. A., Cairns, I. H., & Willes, A. J. 1994, ApJ, 422, 870
Robinson, P. A., Willes, A. J., & Cairns, I. H. 1993, ApJ, 408, 720
Robinson, R. D. 1977, Sol. Phys., 55, 459
———. 1978, Sol. Phys., 56, 405
———. 1983, Proc. Astron. Soc. Australia, 5, 208
Roelof, E. C., & Pick, M. 1989, A&A, 210, 417
Rosenberg, H. 1975, Sol. Phys., 42, 247
Smerd, S. F., Wild, J. P., & Sheridan, K. V. 1962, Australian J. Phys., 15, 180
Steinberg, J. L., Aubier-Giraud, M., Leblanc, Y., & Boischot, A. 1971, A&A, 10, 362
Stewart, R. T. 1972, Proc. Astron. Soc. Australia, 2, 100
———. 1974a, in IAU Symp. 57, Coronal Disturbances, ed. G. Newkirk, Jr. (Dordrecht: Reidel), 161
———. 1974b, Sol. Phys., 39, 451
Suzuki, S., & Dulk, G. A. 1985, in Solar Radiophysics, ed. D. J. McLean & N. R. Labrum (New York: Cambridge Univ. Press), 289
Weiss, A. A., & Stewart, R. T. 1965, Australian J. Phys., 18, 145
Wild, J. P., Murray, J. D., & Rowe, W. C. 1954, Australian J. Phys., 7, 439
Wild, J. P., Sheridan, K. V., & Neyland, A. A. 1959a, Australian J. Phys., 12, 369
Wild, J. P., Sheridan, K. V., & Trent, G. H. 1959b, in IAU Symp. 9, URSI Symp. 1, Paris Symposium on Radio Astronomy, ed. R. N. Bracewell (Stanford: Stanford Univ. Press), 176
Willes, A. J., Robinson, P. A., & Melrose, D. B. 1996, Phys. Plasmas, 3, 149
Wu, C. S. 1968, Phys. Fluids, 11, 1733
Wu, C. S., Li, Y., & Yoon, P. H. 2000a, in Radio Astronomy at Long Wavelengths, ed. R. G. Stone, K. W. Weiler, M. L. Goldstein, & J.-L. Bougeret (Washington, DC: AGU), 47
Wu, C. S., Yoon, P. H., & Li, Y. 2000b, ApJ, 540, 572
Wu, C. S., Yoon, P. H., & Zhou, G. C. 1994, ApJ, 429, 406
Yoon, P. H. 1995, Phys. Plasmas, 2, 537
———. 1997, Phys. Plasmas, 4, 3863
———. 1998, Phys. Plasmas, 5, 2590
Yoon, P. H., Weatherwax, A. T., & Rosenberg, T. J. 1998, J. Geophys. Res., 103, 4071
Yoon, P. H., & Wu, C. S. 1994, Phys. Plasmas, 1, 76
Zheleznyakov, V. V. 1970, Radio Emission of the Sun and Planets (New York: Pergamon)
Zirin, H. 1966, The Solar Atmosphere (Waltham: Blaisdell)